Defence Science Journal, Vol. 60, No. 6, November 2010, pp. 628-638

REVIEW PAPER

Computational Elements for High-fidelity Aerodynamic Analysis and Design Optimisation

Chongam Kim

Seoul National University, Seoul–151 744, Korea
Email: chongam@snu.ac.kr

ABSTRACT

The study reviews the role of computational fluid dynamics (CFD) in aerodynamic shape optimisation, and discusses some of the efficient design methodologies. The article in the first part, numerical schemes required for high-fidelity aerodynamic flow analysis are discussed. To accurately resolve high-speed flow physics, high-fidelity shock-stable schemes as well as intelligent limiting strategy mimicking multi-dimensional flow physics are essential. Exploiting these numerical schemes, some applications for 3-D internal/external flow analyses were carried out with various grid systems which enable the treatment of complex geometries. In the second part, depending on the number of design variables and the way to obtain sensitivities or design points, several global and local optimisation methods for aerodynamic shape optimisation are discussed. To avoid the problem that solutions of gradient-based optimisation method, (GBOM) are often trapped in local optimum, remedy by combining GBOM with global optimum strategy, such as surrogate models and genetic algorithm (GA) has been examined. As an efficient grid deformation tool, grid deformation technique using NURBS function is discussed. Lastly, some 3-D examples for aerodynamic shape optimisation works based on the proposed design methodology are presented.

Keywords: Aerodynamic shape optimisation, high-fidelity numerical methods, gradient-based optimisation method, meta modelling, genetic algorithm, adjoint variable method, aerodynamic analysis.

1. INTRODUCTION

In the past, many engineering design problems were tried to be solved largely by trial and error depending on engineers' experience and intuition. Thus, a lot of manpower, time or cost was inevitable to obtain an aerodynamically optimal shape. Nowadays, keeping pace with the rapid growth of computing power, commercial software replaces engineers' efforts in the field of aircraft design, such as 3-D geometric modelling, structure analysis, and flow computations. Computational software also contributes in reducing errors caused by human factors, such as incomplete knowledge based on poor experience, mental and/or physical fatigue. However, unlike CAD and FEM-based structural analysis software, reliability and commercialisation of CFD software still relatively stays at low level, nevertheless considerable efforts to develop advanced CFD methods. In general, it requires hundreds of flow solutions to complete a reliable aerodynamic optimisation process. For that reason, flow analysis and aerodynamic design optimisation techniques must be carefully devised or selected by optimising the trade-off between numerical accuracy and computational efficiency. Assuming that the computing power steadily grows, the paper reviews literature on some essential elements required for high-fidelity aerodynamic flow analysis and design optimisation. Design methodology based on Euler or Navier-Stokes equations can be roughly classified into gradient and non-gradient methods depending on the usage of sensitivity analysis process. Non-gradient optimisation method is mostly a kind of global optimisation method, while gradient-based method is local optimisation method. Each optimisation approach has its own merits and demerits depending on design problems. Generally, computational aerodynamic shape optimisation consists of the four essential elements: (i) flow solver, (ii) sensitivity analysis solver (in case of gradient-based optimisation), (iii) grid generator (or grid modifier), and (iv) optimisation algorithm[1].

Among the four elements, an accurate and efficient flow solver is the first concern because it provides flow field information and integral aerodynamic loads such as lift or drag, which are intrinsic ingredients of objective function. To obtain robust and reliable flow field information, high-fidelity numerical schemes that are able to resolve complex flow phenomena, are thus the foremost. From this perspective, high-fidelity shock-stable schemes, such as RoeM and AUSMPW+ have been examined[2,3]. RoeM scheme, based on the Roe's approximate Riemann solver, is a shock-stable scheme without any tunable parameters while maintaining the accuracy of the original Roe scheme[2]. AUSMPW+ scheme is an improved version of AUSMPW scheme. Using pressure-based weighting functions, AUSMPW+ can reflect both physical properties across a cell interface adequately. As a result, oscillations and overshoots behind shocks

Received 08 April 2010, Revised 15 July 2010

and near a wall, which are typical symptoms of AUSM-type schemes, are successfully eliminated. Both RoeM and AUSMPW+ schemes are among the recently developed advanced numerical fluxes for gas dynamics. In addition, to achieve high-order spatial accuracy by incorporating multi-dimensional flow physics, multi-dimensional limiting process (MLP) are discussed in 2-D and 3-D setting[4-6].

The sensitivity analysis method commonly used can be summarised by four techniques, (i) finite difference method (FDM)[7], (ii) direct differentiation (DD)[8], (iii) complex step derivative[9], and (iv) continuous/discrete adjoint variables[7,10]. Among them, adjoint variable approaches are most popular since computational cost is almost independent of the number of design variables and roughly the same as the cost of flow analysis. Thus, adjoint method is particularly useful in the problems with many design variables. In the present work, sensitivity analysis by discrete adjoint approach has been examined. Furthermore, the extension of the adjoint approach to various grid systems, such as multi-block for internal flow application and overset mesh system for multiple-body external problem has been discussed.

Regarding the geometric modification required in shape optimisation process, various shape functions have been used. Smoothness in shape change and a flexible degree of freedom (DOF) in design space are the top priorities in choosing a shape function. For that reason, a non-uniform rational B-spline (NURBS) equation can be employed as a new shape function, and the control points of NURBS surface are then used as design variables. NURBS can maintain grid smoothness since NURBS equations can preserve a certain level of higher-order derivatives at each knot of the surface. Hence, gradient smoothing affecting the accuracy of sensitivity can no longer be necessary.

Lastly, as an optimisation strategy to avoid the potential danger, that solutions of GBOM are often trapped in local optimum in highly nonlinear design space, an efficient approach by combining surrogate models and genetic algorithm (GA) has been examined. Exploiting all of the elements for the high-fidelity flow analysis and ASO, some three-dimensional design works including inlet and wing/body design have been presented.

2. NUMERICAL SCHEMES FOR FLOW ANALYSIS

For compressible flow analysis, a numerical design of inviscid fluxes, namely a numerical flux function at a cell-interface, should guarantee a high level of accuracy, efficiency, and robustness. Upwind-basing is the most physical approach to capture various linear and nonlinear waves, which can be categorised as either flux difference splitting (FDS) or flux vector splitting (FVS) schemes. FDS schemes are based on the idea of Godunov, and the Riemann problem is used locally. Many researchers have tried to simplify the step of numerical flux calculation, which leads to the family of Godunov-type schemes or approximate Riemann solvers, such as Roe's FDS, HLLE(M), Osher's FDS, and so on. FVS, such as van Leer's and other variants, has advantages in view of robustness and efficiency. At the same time, it is also well-known that these schemes suffer accuracy problems in resolving shear layer region due to excessive numerical dissipation. On the other hand, AUSM-type schemes, originally proposed by Liou, *et al.*, turn out to be advantageous in several aspects.

In an effort to improve the accuracy and robustness of previous numerical flux schemes, several high-fidelity flux schemes such as RoeM[2], AUSMPW+[3] are designed. As the same time, multi-dimensional limiting process (MLP)[4-6] is also proposed to achieve high-order spatial accuracy and to incorporate multi-dimensional effect. Exploiting these numerical schemes, reliable two- and three-dimensional internal/external flow analyses can be carried out with various grid systems. However, the accuracy of high-speed aerodynamic simulation is always limited by computational burden, because high-fidelity simulation usually means high computational cost, and thus a slow design cycle. Therefore, appropriate set of additional numerical strategies has to be chosen for high Reynolds number flow design considering computational efficiency and numerical accuracy:

- First, efficient time integration technique to reduce computational cost, such as multi-grid with residual smoothing or GMRES.
- Second, adequate turbulence modelling for separated flows, such as S-A or *k-w* SST model.
- Third, grid system to capture delicate flow phenomena especially in boundary layer around 3-D realistic configuration, such as overset mesh system.

2.1 RoeM

RoeM[2] scheme is an improved Roe-type scheme that is free from the shock instability and still preserves the accuracy and efficiency of the original Roe's FDS[11]. Roe's FDS is known to possess good accuracy but suffers from the shock instability, such as the carbuncle phenomenon. As the first step towards a shock-stable scheme, Roe's FDS is compared with the HLLE scheme to identify the source of the shock instability. Through a linear perturbation analysis of the odd-even decoupling problem, damping characteristic was examined and Mach number-based functions *f* and *g* were introduced to balance damping and feeding rates, which leads to a shock-stable Roe scheme. To satisfy the conservation of total enthalpy, which is crucial in predicting surface heat transfer rate in high-speed steady flows, an analysis of dissipation mechanism in the energy equation was carried out to find the error source and to make the proposed scheme preserve the total enthalpy. Modifying the maximum-minimum wave speed, the problem of expansion shock and numerical instability in the expansion region could also be remedied without sacrificing the exact capturing of contact discontinuity. From these analyses, the newly formulated RoeM scheme is proposed as follows:

$$F_{j+1/2} = \frac{b_1 \times F_j - b_2 \times F_{j+1}}{b_1 - b_2} + \frac{b_1 \times b_2}{b_1 - b_2}\Delta Q^* - g\frac{b_1 \times b_2}{b_1 - b_2} \times \frac{1}{1+\left|\hat{M}\right|} B\Delta Q \quad (1)$$

$$\Delta Q^* = \begin{pmatrix} \rho \\ \rho u \\ \rho v \\ \rho H \end{pmatrix}, \quad B\Delta Q = \left(\Delta\rho - f \frac{\Delta p}{\hat{c}^2} \right) \begin{pmatrix} 1 \\ \hat{u} \\ \hat{v} \\ \hat{H} \end{pmatrix} + \rho \begin{pmatrix} 0 \\ \Delta u - n_x \Delta U \\ \Delta v - n_y \Delta U \\ \Delta H \end{pmatrix} \tag{2}$$

$$b_1 = \max(0, \hat{U} + \hat{c}, U_{j+1} + \hat{c}), \quad b_2 = \min(0, \hat{U} - \hat{c}, U_j - \hat{c}) \tag{3}$$

where

$$f = \begin{cases} 1, & \hat{u}^2 + \hat{v}^2 = 0 \\ \left| \hat{M} \right|^h, & \text{elsewhere} \end{cases} \tag{4}$$

$$h = 1 - \min(P_{i,j+(1/2)}, P_{i-(1/2),j}, P_{i-(1/2),j+1}, P_{i+(1/2),j+1}) \tag{5}$$

$$P_{i,j+(1/2)} = \min\left(\frac{p_{i,j}}{p_{i+1,j}}, \frac{p_{i,j+1}}{p_{i,j}} \right) \tag{6}$$

and

$$g = \begin{cases} \left| \hat{M} \right|^{1-\min\left(\frac{p_j}{p_{j+1}}, \frac{p_{j+1}}{p_j} \right)}, & \hat{M}^2 \neq 0 \\ 1, & \hat{M}^2 = 0 \end{cases} \tag{7}$$

2.2 AUSMPW+

Typical symptoms appearing in the application of AUSM-type schemes in high-speed flows, such as pressure wiggles near a wall and overshoots across a strong shock, can be cured by introducing weighting functions based on pressure (AUSMPW)[12]. The main feature of AUSMPW is the removal of the oscillations of AUSM+ near a wall or across a strong shock by introducing pressure-based weight functions. AUSMPW uses the pressure-based weight function f to treat the oscillations near a wall and w to remove the oscillation across a strong shock. The starting point of AUSMPW is to observe the fact that AUSM+ and AUSMD are complementary to each other. AUSM+ considers the left cell density only while AUSMD takes both cell densities. This may be the reason for the numerical oscillations of AUSM+ and carbuncle phenomena of AUSMD.

Thus, by incorporating the property of the right cell p_R, numerical oscillations near a wall can be eliminated. A newly improved version of the AUSMPW scheme[3], called AUSMPW+, is developed to increase the accuracy and computational efficiency of AUSMPW in capturing oblique shock without compromising robustness. With a new definition of numerical speed of sound at a cell interface, oblique shock can be captured accurately, and it can be proved that AUSMPW+ completely excludes unphysical expansion shock[3]. The AUSMPW+ flux at a cell interface can be summarised as

$$F_{\frac{1}{2}} = \bar{M}_L^+ C_{\frac{1}{2}} \Phi_L + \bar{M}_R^- C_{\frac{1}{2}} \Phi_R + \left(P_L^+ \big|_{\alpha=\frac{3}{16}} P_L + P_R^- \big|_{\alpha=\frac{3}{16}} P_R \right) \tag{8}$$

$$\begin{aligned} &\text{if } m_{1/2} \geq 0, \\ &\quad \bar{M}_L^+ = M_L^+ + M_R^- \cdot \left[(1-\omega) \cdot (1 + f_R) - f_L \right] \\ &\quad \bar{M}_R^- = M_R^- \cdot \omega \cdot (1 + f_R) \\ &\text{elseif } m_{1/2} \leq 0, \\ &\quad \bar{M}_L^+ = M_L^+ \cdot \omega \cdot (1 + f_L) \\ &\quad \bar{M}_R^- = M_R^- + M_L^+ \cdot \left[(1-\omega) \cdot (1 + f_L) + f_L - f_R \right] \end{aligned} \tag{9}$$

with $\omega(p_L, p_R) = 1 - \min\left(\frac{p_L}{p_R}, \frac{p_R}{p_L} \right)^3$. $f_{L,R}$ is simplified as

$$f_{L,R} = \begin{cases} \left(\frac{p_{L,R}}{p_s} - 1 \right) \min\left(1, \frac{\min(p_{1,L}, p_{1,R}, p_{2,L}, p_{2,R})}{\min(p_L, p_R)} \right)^2, & p_s \neq 0 \\ 0, & \text{elsewhere} \end{cases} \tag{10}$$

where $p_s = P_L^+ p_L + P_R^- p_R$, and the Mach number and pressure splitting functions of AUSMPW+ at a cell interface are as follows.

$$M^{\pm} = \begin{cases} \pm \frac{1}{4} (M \pm 1)^2, & |M| \leq 1 \\ \frac{1}{2} (M \pm |M|), & |M| > 1 \end{cases} \tag{11}$$

$$P^{\pm}\big|_{\alpha} = \begin{cases} \pm \frac{1}{4} (M \pm 1)^2 (2 \mp M) \pm \alpha M \left(M^2 - 1 \right)^2, & |M| \leq 1 \\ \frac{1}{2} (1 \pm sign(M)), & |M| > 1 \end{cases} \tag{12}$$

2.3 Multi-dimensional Limiting Process

Since the late 1970s, numerous ways to control oscillations have been studied and several limiting concepts have been proposed. Most representatives would be TVD[13,14], TVB[15], and ENO/WENO[16,17]. Most oscillation-free schemes have been largely based on the mathematical analysis of one-dimensional convection equation, and applied to multi-dimensional applications with dimensional splitting. They are successful in many cases, but quite often, it is insufficient or almost impossible to control oscillations near shock discontinuity in multiple dimensions. This manifests the necessity to design oscillation control method for multi-dimensional flow physics.

By extending the one-dimensional monotonic condition to 2-D and 3-D flows, the multi-dimensional limiting condition is proposed, and with this limiting condition, the multi-dimensional limiting process (MLP)[4-6] can be formulated. The starting point is the observation that the dimensional splitting extension does not possess any information on property distribution at cell vertex points, whose information is essential when property gradient is not aligned with local grid lines. To derive the multi-dimensional limiting function, the vertex point value is expressed in terms of

variations across cell-interface, and then, they determine the variation to satisfy the multi-dimensional limiting condition using the limiting coefficient α. The coefficient α possesses the information of multi-dimensionally distributed physical property. With the coefficient α, the multi-dimensional limiting function can be formulated. Finally, a new family of limiters to control oscillations in multi-dimensional flows can be developed. For a 3-D flow,

$$\begin{aligned}\Phi^{L}_{i+1/2,j,k} &= \bar{\Phi}_{ijk} + 0.5\phi\left(r^{\xi}_{L,i,j,k},\alpha_L,\beta_L\right)\Delta\Phi_{i-1/2,j,k}\\ \Phi^{R}_{i+1/2,j,k} &= \bar{\Phi}_{ijk} - 0.5\phi\left(r^{\xi}_{R,i,j,k},\alpha_R,\beta_R\right)\Delta\Phi_{i+3/2,j,k}\end{aligned} \tag{13}$$

where α is the multi-dimensional restriction coefficient which determines the baseline region of MLP, and β is the local slope evaluated by a higher-order polynomial interpolation. The interpolated values of $\Phi^{L}_{i+1/2,j,k}$ and $\Phi^{R}_{i+1/2,j,k}$ are based on the final form of MLP. Since the calculations of interpolated values are independent of a numerical flux, MLP can be combined with any numerical flux. $\alpha_{L,R}$ and $\beta_{L,R}$ in Eqn. (13) can be summarised as follows.

Along the ξ-direction, if $\Delta\Phi^{p}_{\xi} \geq 0$,

$$\begin{aligned}\alpha_L &= g\left[\frac{2\max(1,\gamma^{\xi}_{L,i,j,k})(\bar{\Phi}^{\max}_{p,q,r}-\bar{\Phi}_{i,j,k})}{\left(1+\dfrac{\Delta\Phi^{q}_{\eta}}{\Delta\Phi^{q}_{\xi}}+\dfrac{\Delta\Phi^{\gamma}_{\xi}}{\Delta\Phi^{p}_{\xi}}\right)_{i,j,k}\Delta\Phi_{i+1/2,j,k}}\right],\\ \alpha_R &= g\left[\frac{2\max(1,\gamma^{\xi}_{R,i,j,k})(\bar{\Phi}^{\min}_{p,q,r}-\bar{\Phi}_{i,j,k})}{\left(1+\dfrac{\Delta\Phi^{q}_{\eta}}{\Delta\Phi^{q}_{\xi}}+\dfrac{\Delta\Phi^{\gamma}_{\xi}}{\Delta\Phi^{p}_{\xi}}\right)_{i+1,j,k}\Delta\Phi_{i+3/2,j,k}}\right]\end{aligned} \tag{14}$$

where $r^{\xi}_{L,i,j,k}=\dfrac{\Delta\Phi_{i+1/2,j,k}}{\Delta\Phi_{i-1/2,j,k}}$, $r^{\xi}_{R,i,j,k}=\dfrac{\Delta\Phi_{i+1/2,j,k}}{\Delta\Phi_{i+3/2,j,k}}$

and $g(x)=\max\left(1,\min\left(2,x\right)\right)$.

Along the η- and ξ-direction, the left and right values at the cell interface can be calculated in the same way. With β in the form of a third-order polynomial and a fifth-order polynomial, they finally obtain MLP3 and MLP5, respectively. For detailed explanation, Fig. 1 shows the computed results of shock-vortex interaction[4-6]. Compared to conventional limiting, MLP can control oscillations across the shock discontinuity and capture local flow structure in detail.

3. AERODYNAMIC SHAPE OPTIMISATION

Though the progress of computing environment makes the choice of optimisation methods flexible, a design strategy has to be judiciously chosen by considering the characteristics of design problems. Global optimisation method may provide the global optimum value within the specified design space. For example, GA originated from the theory of natural evolution is widely used as a global optimisation tool[18-20] but it is generally costly in imitating an accurate evolutional process. Particularly for 3-D aerodynamic design problems with a lot of design variables, it requires an enormous amount of computational time in evaluating experimental data at each design point. Thus, some approximation, called meta-modelling originated from statistics, is popularly adopted, such as RSM[21,22] or Kriging[23,24]. These modelling methods may still require a huge computational cost to obtain sufficient experimental data for building up the response model, if geometric shape is complex or the number of design variable is large. Furthermore, if sample experimental points representing objective function values are not appropriate, design results can be poorer than other optimisation tools. As an improved meta-modelling, optimisation based on Kriging model is applied for the robust exploration of the global optimum value. Jones[25], *et al.* firstly introduced the expected improvement method originally proposed by Mockus[26], *et al.* into Kriging model.

Adjoint approach based gradient-based optimisation method is also popular among local optimisation methods because computational cost is essentially independent of the number of design variables. In addition, it exhibits a good convergence characteristic because GBOM uses the gradient vector of the objective function which usually provides an optimal direction in design space. It is particularly powerful in case of wing surface design with a lot of design variables. Jameson[10,27,28], *et al.* proposed continuous adjoint approach, and applied it to aerodynamic shape optimisation problems of various wing/body geometries with wing planform and surface design variables. Lee[29], *et al.* extended the discrete adjoint method to overset mesh system, which can be applied to complex geometries with a relatively simple grid topology. Through these applications, continuous or discrete adjoint variable methods have demonstrated the capability to produce

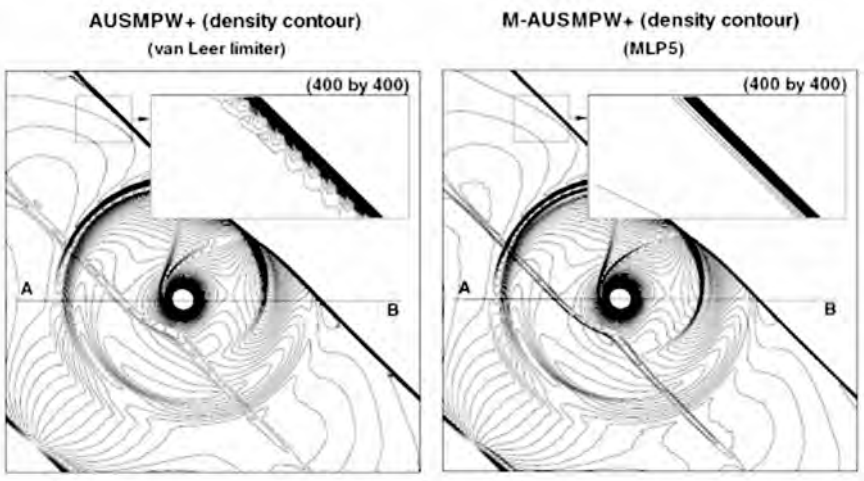

Figure 1. Comparison of density distributions for shock wave-vortex interaction.

a substantial improvement of aerodynamic performance. Despite the superior performance in aerodynamic design problems, GBOM has a potential danger to be trapped in local optimum during design process, especially in cases of noisy nonlinear design spaces.

3.1 Genetic Algorithm

Genetic algorithm is a class of stochastic algorithm inspired by natural evolution, and has been applied to find optimum values in various fields. Starting with a randomly generated population of chromosomes, a GA goes through a process of fitness-based selection and recombination to produce successor population or the next generation. During recombination, parent chromosomes are selected and their genetic material is recombined to generate the child generation. As this process is progressed iteratively, a sequence of successive generations evolves and average fitness of the chromosomes tends to increase until stopping criterion is reached. In this way, a GA evolves into the best solution to a given design problem. An advantage of GA is that, unlike other optimisation algorithms, it does not need gradient information. Therefore, if there are many local extrema and discontinuous properties in objective functions and constraints, GA is more suitable in finding the global optimisation point and design variable set than gradient-based optimisation methods. At the same time, a GA requires substantial computational cost because of a large number of function evaluations. For that reason, it is prohibitive to directly apply it to complex aerodynamic shape optimisation with a large number of design variables.

3.2 Kriging Model

Meta-modelling techniques are commonly used to create approximation of the mean and variation of response in noisy design space. A meta-model is adopted as a surrogate approximation for actual experimental data or numerical analysis during design process. Among the meta-modelling techniques, RSM and Kriging model are the most popular techniques in aerodynamic shape design. RSM employs a simple polynomial function using the least square regression technique. For that reason, RSM has a limitation if physical phenomena are highly nonlinear or noisy wrt design variables. Kriging method is more flexible in dealing with aerodynamic design problems of highly nonlinear design space[23-26]. Kriging method was developed in the field of geo-statistics, and it is useful in predicting correlated data temporally and spatially. A most distinguished advantage of Kriging model is that it can exactly interpolate sample data, and can represent a function with multiple local extrema.

3.3 Expected Improvement

Once a Kriging model is constructed, GA is used to search the global optimum value within the specified design space. Thus, there is a possibility that the global optimum value given by GA may not be the global optimum in the real design space. As a way to find more accurate response surface and more efficient exploration for global optimum point, expected improvement has been proposed[25,26].

The main idea is that the uncertainty of the predicted value should be taken into account in sampling additional point for the initial Kriging model. In this process, expected improvement basically provides a kind of figure of merit (or a value of expected improvement) when additional sample point is added to the existing sample data. For example, during the minimising process of objective function, expected improvement can be formulated and expressed in a closed form as in Eqns. (15) and (16).

$$I(x)=\begin{cases} f_{\min}-\hat{y}(x), \; if \;\; \hat{y}<f_{\min} \\ 0 \qquad\qquad\quad ,\text{otherwise} \end{cases} = \max\left[f_{\min}-\hat{y}(x),0\right] \quad (15)$$

$$E\left[I(x)\right]=(f_{\min}-\hat{y})\Phi\left(\frac{f_{\min}-\hat{y}}{s}\right)+s\varphi\left(\frac{f_{\min}-\hat{y}}{s}\right) \quad (16)$$

where $f_{\min}$ is the current minimum value obtained by flow solver and $\hat{y}$ is predicted by the Kriging model, s is the root mean square error of the predictor representing some uncertainty at the predicted point, Φ and ϕ are the normal distribution and normal density function, respectively. From Eqn. (16), the maximum expected improvement point can be evaluated, and the value of the sample point obtained by CFD solver is added. If the objective function value of the sample point is smaller than the current minimum value, is newly updated. This process is iteratively performed and stopped until the expected improvement becomes less than some threshold criterion. Through the Kriging-expected improvement process, the point nearer the global optimum can be predicted in the specified design space[23-25].

3.4 Sensitivity Analysis-based on Discrete Adjoint Approach

Discrete adjoint variable method is applied to get sensitivity information by fully hand differentiating the three-dimensional Euler and N-S equations. The symbolic formulation of the discrete residual R for the steady-state flow equations can be written as

$$\{R\}=\{R(Q,X,D)\}=\{0\} \quad (17)$$

where Q is the flow variable vector, X is the position of computational grid and D is the vector of design variables. Without evaluating the vector dQ/dD, the sensitivity derivative of the objective function, $F = F(Q,X,D)$, can be calculated as

$$\left\{\frac{dF}{dD}\right\}=\left\{\frac{\partial F}{\partial Q}\right\}^T\left\{\frac{dQ}{dD}\right\}+\left\{\frac{\partial F}{\partial X}\right\}^T\left\{\frac{dX}{dD}\right\}+\left\{\frac{\partial F}{\partial D}\right\} +\Lambda^T\left(\left[\frac{\partial R}{\partial Q}\right]\left\{\frac{dQ}{dD}\right\}+\left[\frac{\partial R}{\partial X}\right]\left\{\frac{dX}{dD}\right\}+\left\{\frac{\partial R}{\partial D}\right\}\right) \quad (18)$$

if and only if the adjoint vector Λ satisfies the following adjoint equation.

$$\left\{\frac{\partial F}{\partial Q}\right\}^T+\Lambda^T\left[\frac{\partial R}{\partial Q}\right]=\{0\}^T \quad (19)$$

The solution vector Λ is then obtained by solving Eqn. (19) with the Euler implicit method in a time-iterative manner as

$$\left(\frac{I}{J\Delta t}+\left[\frac{\partial R}{\partial Q}\right]\right)\Delta\Lambda=-\left[\frac{\partial R}{\partial Q}\right]^{T}\Lambda^{m}-\left\{\frac{\partial F}{\partial Q}\right\},$$
$$\Lambda^{m+1}=\Lambda^{m}+\Delta\Lambda \tag{20}$$

where I is the identity matrix, J the Jacobian matrix, and the subscript VL means the van Leer flux Jacobian. Adjoint formulation on the overset boundary can be similarly derived by slightly modifying the conventional adjoint boundary condition, which can be expressed as

$$\left[\frac{\partial R^{M}}{\partial Q^{M}}\right]^{T}\Lambda^{M}+\left[\frac{\partial R_{F}^{S}}{\partial Q^{M}}\right]^{T}\Lambda_{F}^{S}+\left\{\frac{\partial F^{M}}{\partial Q^{M}}\right\}^{T}=\{0\}^{T} \tag{21}$$

$$\left[\frac{\partial R^{S}}{\partial Q^{S}}\right]^{T}\Lambda^{S}+\left[\frac{\partial R_{F}^{M}}{\partial Q^{S}}\right]^{T}\Lambda_{F}^{S}+\left\{\frac{\partial F^{M}}{\partial Q^{M}}\right\}^{T}=\{0\}^{T} \tag{22}$$

$$\left[\frac{\partial R^{M}}{\partial Q_{F}^{M}}\right]^{T}\Lambda^{M}+\left[\frac{\partial R_{F}^{M}}{\partial Q_{F}^{M}}\right]^{T}\Lambda_{F}^{M}+\left\{\frac{\partial F^{M}}{\partial Q_{F}^{M}}\right\}^{T}=\{0\}^{T} \tag{23}$$

$$\left[\frac{\partial R^{S}}{\partial Q_{F}^{S}}\right]^{T}\Lambda^{S}+\left[\frac{\partial R_{F}^{S}}{\partial Q_{F}^{S}}\right]^{T}\Lambda_{F}^{S}+\left\{\frac{\partial F^{S}}{\partial Q_{F}^{S}}\right\}^{T}=\{0\}^{T} \tag{24}$$

where the subscript F indicates fringe cell. The superscript M and S represents the main-grid and sub-grid domain, respectively. By solving the four equations sequentially, overset boundary value on the main- and sub-grid can be updated. The update procedure of the adjoint variables on the overset boundary Eqns. (21) to (24) is reverse to the conventional overset flow analysis because of the transposed operation in the adjoint formulation.

3.5 Geometric Modification–NURBS

In automatic shape design for 3-D geometry, a grid generator, which guarantees a sufficient and flexible design space, is important. NURBS surface equations can be employed as new shape functions. The benefits of NURBS have already been mentioned and the determination of control points and NURBS blending functions, grid generation process from the evaluated NURBS equations are discussed. The coordinate vectors of NURBS curve, $X(u)$, are expressed by

$$X(u)=\frac{\Sigma_{i=0}^{n}h_{i}P_{i}N_{i,k}(u)}{h} \tag{25}$$

where homogeneous coordinate h represents

$$h=\sum_{i=0}^{n}h_{i}N_{i,k}(u) \tag{26}$$

and $P_i=(x_i,y_i,z_i)$ is a position vector of the i^{th} control point in 3-D space. Homogeneous coordinate acts as a weighting factor for each control point. As the value of h increases, the corresponding NURBS curve is closer to the control point. To impose equal weighting for each control point, all the homogeneous coordinates can be set to *1*. The value of n indicates the number of control point. Also, blending functions are defined as

$$N_{i,k}(u)=\frac{(u-t_{i})N_{i,k-1}(u)}{t_{i+k}-t_{i}}+\frac{(t_{i+k+1}-u)N_{i+1,k-1}(u)}{t_{i+k+1}-t_{i+1}},$$
$$N_{i,0}(u)=\begin{cases}1 & (t_{i}\le u\le t_{i+1})\\ 0 & \text{otherwise}\end{cases} \tag{27}$$

where t_i (i = 0, 1, 2, . . .) are knot-values, and subscript k indicates the order of NURBS blending function[30].

The grid points are approximated by the least-square method with NURBS. After this, control points and homogeneous coordinates (weighting factors) can be used as design variables. The grid sensitivity is then finally evaluated as in Eqns. (28) and (29). For the i^{th} control point,

$$\frac{\partial X(u)}{\partial P_{i}}=\frac{h_{i}N_{i,k}(u)}{\Sigma_{i=0}^{n}h_{i}N_{i,k}(u)} \tag{28}$$

And, for the i^{th} weighting factor,

$$\frac{\partial X(u)}{\partial h_{i}}=\frac{N_{i,k}(u)\left[\Sigma_{j=0}^{n}\left\{(P_{i}-P_{j})h_{j}N_{j,k}(u)\right\}\right]}{\left[\Sigma_{i=0}^{n}h_{i}N_{i,k}(u)\right]^{2}} \tag{29}$$

In case of NURBS surface approximation, the overall procedure is similar to NURBS curve approximation except it is formulated by 2-D NURBS equations.

4. DESIGN CASE STUDY

4.1 Turbulent Internal Flow Design

Adjoint approach, which has been very successful in external flow problems, does not seem to be applied to highly viscous internal flow problems yet. This is mainly due to the difficulty in differentiating turbulence transport equations[7]. In addition, awfully time-consuming work in developing a reliable adjoint code may discourage its application to internal flow design problems. Most researches on optimal intake design employs parametric studies, GBOM using finite difference method, or other global optimisation methods based on the modelling of design space. They carry out the design optimisation of a subsonic intake based on the discrete adjoint approach. The sensitivity analysis for two-equation turbulence model is performed to allow a large number of design variables and to globally modify the intake (or duct) geometry. The computational cost involved in two adjoint equations for turbulence transport equations is side-stepped by the parallelised adjoint method[31]. As a result, the computational cost for sensitivity analysis with the parallelised adjoint method is almost equal to that of the flow solver.

The objective function is to maximise the total pressure recovery with minimising the loss of other performance measures. The maximisation of the volume-averaged total pressure (VATP) is adopted as a useful objective function. The VATP is defined by

$$VATP = \int_V P_0 dv / \int_V dv \qquad (30)$$

where $\int_V$ implies the volume integration from (x/D = 0) (D: throat diameter) to the outlet boundary, and P_0 is the total pressure in the duct.

Figure 2 shows the geometric change between the baseline model and the designed model. The duct geometry after design is somewhat beyond expectation, and it appears that this kind of shape change can rarely be obtained from conventional design works. Intuitively, three noticeable features can be observed from Fig. 2. as follows:

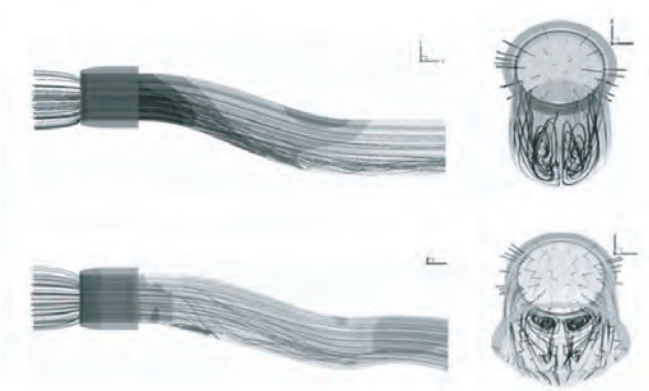

Figure 2. Streamline comparison (VATP maximisation, Up: baseline, Down: designed).

- Firstly, curved region at the lower surface is stretched after design. As a result, the suction effect at the lower surface becomes weak and the size of flow separation is remarkably reduced.
- Secondly, the exhaust region of the designed intake is changed into an elliptical shape from a circular section. This reduces the intensity of swirling flow over the whole duct region.
- Lastly, a smooth bump appears along the lower surface near the exhaust region, which stabilises flow into the engine face.

The performance of the VATP designed model is examined at several off-design conditions. The performance coefficients of the baseline and designed geometry are compared by changing the mass flow rate into the engine. For each design case, total pressure recovery, distortion and mass flow rate are compared under the same free-stream conditions and also under the back pressure condition. It is observed that the designed model shows a better performance than the baseline model in all the off-design test cases.

Through design and off-design condition tests, the present optimisation approach using a discrete adjoint code and NURBS shape modification tool successfully demonstrates that the designed model exhibits a good performance in various flight conditions. Even if it may not guarantee the globally optimal shape, several tests at off-design conditions confirm that the designed model still yields desirable performance over a wide range of flow conditions.

4.2. Extension to Complicated Overset Mesh System

The overset grid technique possesses several attractive properties which can be beneficial to large scale flow analysis and design optimisation.

At first, the grid topology to represent the deforming grid is relatively simple. Secondly, the movement of the sub-domain grid system or the movement of a local component, such as the movement of engine nacelle along the wing surface, can be readily realised without re-generating grid. Thirdly, a high-quality flow solution can be obtained by a relatively small number of grid points. Finally, the fully automatic grid generation is possible because of the simple grid topology. These characteristics of the overset mesh technique can derive the overall aerodynamic design optimisation process into the final goal, i.e., 'fully automatic aerodynamic design from the CAD models'.

In the present work, the seven block overset mesh system of DLR-F4 wing/body configuration, which was the test geometry in the first Drag Prediction Workshop (DPW-I), has been considered[32]. The total number of mesh point is about 1.22 million. The design conditions are the free-stream Mach number of 0.75 and the angle of attack of 0.0 degree, which corresponds to the cruising condition.

Optimisation is performed using the Broydon-Fletcher-Goldfarb-Shanno (BFGS) variable metric method, which is a kind of non-constrained optimisation technique. As a

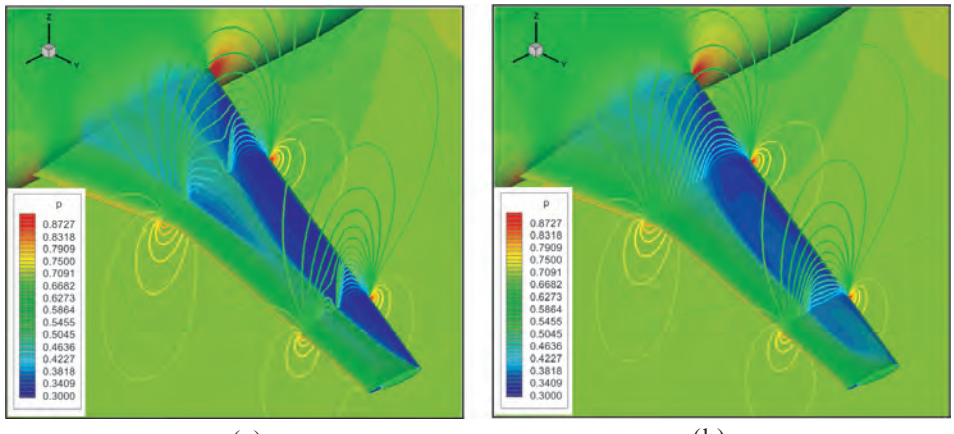

(a) (b)

Figure 3. Comparison of flow pattern between the baseline model and the designed model (Re-design of DLR-F4 wing/body configuration): (a) baseline model (DLR-F4) and (b) designed model.

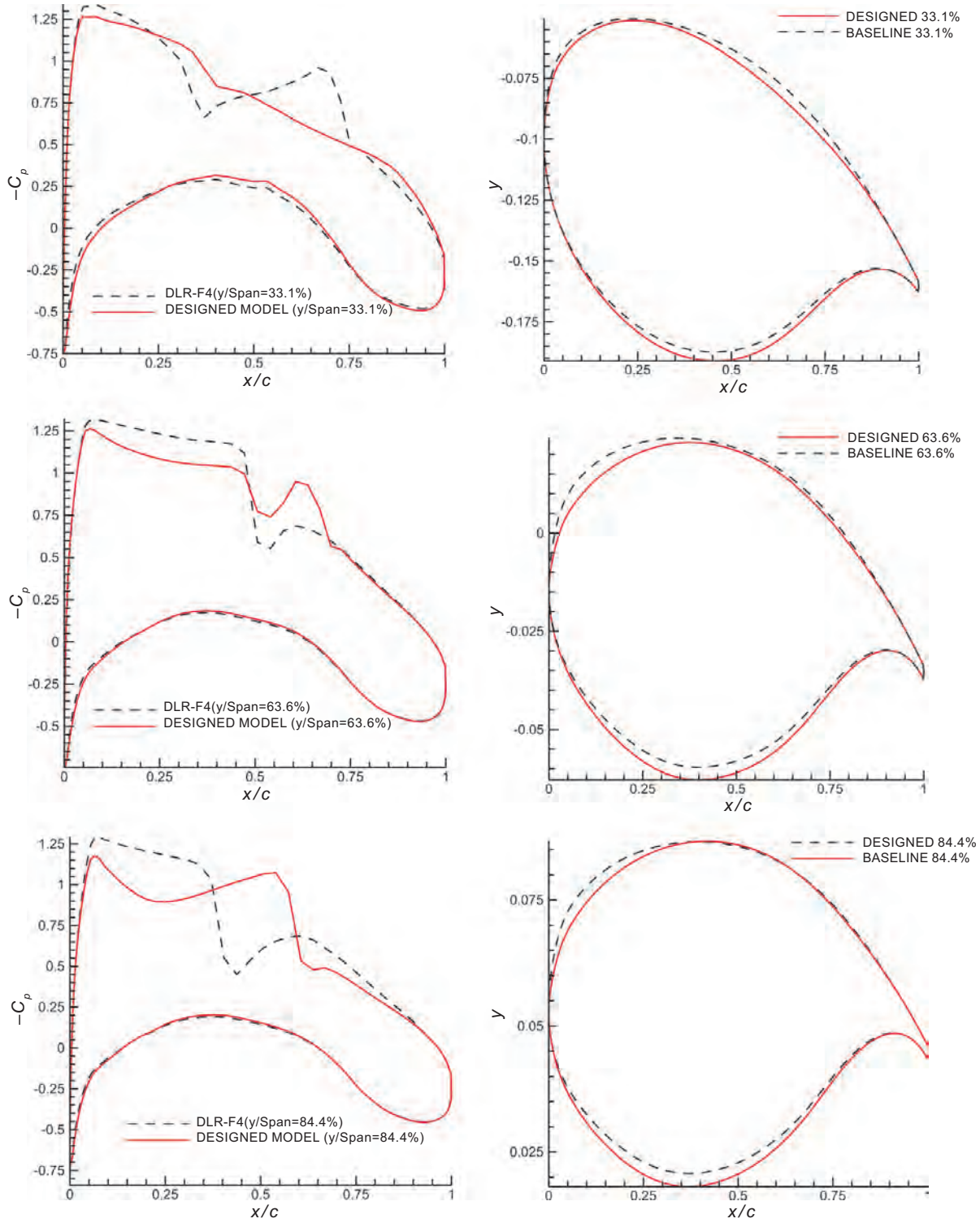

Figure 4. Comparison of C_p curve and geometric change (Re-design of DLR-F4 wing/body configuration).

standard application of the overset GBOM tool, a drag minimisation with maintaining constant lift coefficient is firstly performed. The objective function is defined by Eqn. (33) with the constraint of Eqn. (32). To balance the variation of the penalty function in the objective function, the weighting factor of the lift constraint is given by the ratio of the lift sensitivity to the drag sensitivity wrt angle of attack.

$$\text{Minimise: } C_D \tag{31}$$

$$\text{Subject to: } C_L \geq C_{L_0}, C_{L_0} = \begin{pmatrix}\text{Lift Coefficient of the}\\ \text{Baseline Model}\end{pmatrix} \tag{32}$$

$$F\left(\text{Objective Function}\right) = C_D + Wt \times \min\left[0, C_L - C_{L_0}\right],$$
$$Wt = \frac{\partial C_D}{\partial \alpha} \Big/ \frac{\partial C_L}{\partial \alpha} \tag{33}$$

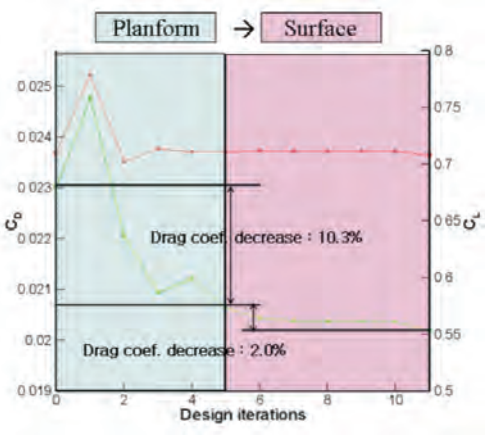

(a)

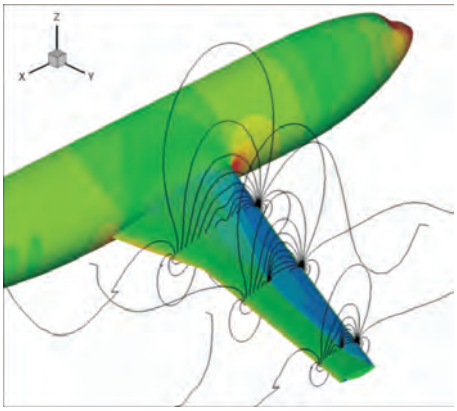

(b)

Figure 5. (a) Two-stage design history, and (b) pressure contour of designed model.

The total number of design variables is 200, located along 10 different design sections of the wing surface. At each design section, 20 Hicks-Henne functions were used. Three component blocks - collar block, wing block, and tipcap block - were overlapped on the wing surface. The deformation of the overlap surface meshes was carried out by the mapping technique from the wing-surface domain to the planform domain.

After design, the drag reduction of the wing only was about 17 per cent, which is quite reasonable considering the drag portion of the fuselage. The *L/D* was changed from 32.26 per cent to 36.25 per cent. It can be observed from Fig. 3 that the shock strength on the wing surface was substantially mitigated after design. At the section of 33 per cent wing span as shown in Fig. 4, the front shock on the upper surface almost disappears because the shelving leading-edge relieves strong expansion.

Regarding the rear shock, the relatively mild slope around x/c = 75 per cent prevents drastic flow expansion after the front shock. The maximum thickness of the wing section is conserved to maintain the lift constraint. As shown at the sections of 84.4 per cent wing span, the position of the maximum thickness along the span-wise direction shifts toward the trailing edge because of the twist angle of the baseline wing. Thus, the flow region after the maximum thickness is not sufficient to transform the rear shock wave into the region of gradual pressure change. Furthermore, the geometric change of the upper wing surface after the maximum thickness region is limited because the wing section gets closer to the wing-tip. This suggests that planform design should be introduced to obtain more refined design solutions such as a shock-free wing. Especially, leading edge sweepback angle can diminish the shock strength on the upper wing surface. Thus planform design variables such as leading edge sweepback, wing span, taper ratio and twist angle are added.

By combining surface design and planform design efficiently, the two-stage design approach is performed[33]. The first stage design is the planform design using global optimisation method based on surrogate model combined with GA. The second stage is the wing surface design through the discrete adjoint approach on overset mesh system. This multi-stage, multi-fidelity design strategy incorporating the discrete adjoint approach and the overset mesh system is certainly expected to provide optimal aerodynamic shape for complex 3-D configurations as in Fig. 5.

5. CONCLUSIONS

Some essential elements required for high-fidelity aerodynamic analysis and design optimisation have been briefly discussed. First of all, AUSMPW+ and RoeM schemes are introduced as accurate, efficient, and robust numerical fluxes for high-fidelity flow analysis. As a multi-dimensional limiting strategy, which ensures multi-dimensional monotonicity and higher-order spatial accuracy, the basic idea of MLP is presented and its performance examined. For the aerodynamic shape design optimisation, various design methods have been discussed depending on the usage of sensitivity analysis process, and the sensitivity analysis technique using discrete adjoint approach is discussed. For robust design optimisation without being trapped in local optimum, multi-stage ASO strategy is employed by combining GBOM for surface design with surrogate models/GA for planform design. Through various 2-D and 3-D applications, the proposed strategy for high-fidelity aerodynamic analysis and design has been verified. However, some challengeable issues for high-fidelity aerodynamic shape optimisation still remain, such as robust convergence of adjoint solver over complex configuration, efficient exploration of highly nonlinear design space, and mesh generation techniques to assure a proper resolution of boundary layers and complex geometries.

ACKNOWLEDGEMENTS

The author appreciates the financial support by National Space Laboratory (NSL) programme through the National Research Foundation of Korea funded by the Ministry of Education, Science and Technology (Grant 20090091724), and by the Korea Science and Engineering Foundation (KOSEF) grant funded by the Korea Government (MEST)

(No.20090084669). The author also appreciates help from Mr JinWoo Yim and Mr JunSok Yi in preparing this manuscript.

REFERENCES

1. Lee, B.J. & Kim, Chongam. Automated design methodology of turbulent internal flow using discrete adjoint formulation. *Aero. Sci. Technol.*, 2007, **11**(2-3), 163-73.
2. Kim, S.S.; Kim, Chongam; Rho, O.H. & Hong, S.K. Cures for the shock instability: development of a shock-stable roe scheme. *J. Comput. Phy.*, 2003, **185**(2), 342-74.
3. Kim, K.H.; Kim, Chongam & Rho, O.H. Methods for the accurate computations of hypersonic flows: Part I. AUSMPW+Scheme. *J. Comput. Phy.*, 2001, **174**(1), 38-80.
4. Kim, K.H. & Kim, Chongam. Accurate, efficient and monotonic numerical methods for multi-dimensional compressible flows: Part II: Multi-dimensional limiting process. *J. Comput. Phy.*, 2005, **208**(2), 570-15.
5. Yoon, S.; Kim, Chongam & Kim, K.H. Multi-dimensional limiting process for three dimensional flow physics analyses. *J. Compu. Phy.*, 2008, **227**(12), 6001-43.
6. Park, Jin Seok; Yoon, Sung-Hwan & Kim, Chongam. Multi-dimensional limiting process for hyperbolic conservation laws on unstructured grids. *J. Comput. Phy.*, 2010, **229**(3), 788-812.
7. Kim, C.S.; Kim, Chongam & Rho, O.H. Sensitivity analysis for the Navier-Stokes equations with two-equation turbulence models. *AIAA Journal*, 2001, **39**(5), 838-45.
8. Eleshaky, M.E. & Baysal, O. Aerodynamic shape optimization using sensitivity analysis on viscous flow equations. *J. Fluid Eng.*, 1993, **115**(3), 75-84.
9. Martins, J.R.R.A.; Kroo, I.M. & Alonso, J.J. Van automated method for sensitivity analysis using complex variables. AIAA Paper 2000-0869, 2000.
10. Leoviriyakit, K.; Kim, S. & Jameson, A. Viscous aerodynamic shape design optimization of wings including planform variables. AIAA Paper-2003-3498, 2003.
11. Roe, P.L. Approximate riemann solvers, parameter vectors and difference schemes. *J. Comput. Phy.*, 1981, **43**(2), 357-72.
12. Kim, K.H.; Lee, J.H. & Rho, O.H. An Improvement of AUSM Schemes by introducing the pressure-based weight functions. *Computers and Fluids*, 1998, **3**, 131-36.
13. Harten, High-resolution schemes for hyperbolic conservation laws. *J. Comput. Phy.*, 1983, **49**(3), 357-93.
14. Sweby, P.K. High-resolution schemes using flux limiters for hyperbolic conservation laws. *SIAM J. Num. Anal.*, 1983, **21**(5), 995-1011.
15. Shu, C.W. TVB uniformly high-order schemes for conservation laws. *Mathematics of Computation*, 1987, **49**(179), 105-21.
16. Shu, C.W. & Osher,S. Efficient implementation of essentially non-oscillatory shock-capturing schemes. *J. Comput. Phy.*, 1988, **77**, 439-71,
17. Liu, X.D.; Osher, S. & Chan, T. Weighted essentially non-oscillatory scheme. *J. Comput. Phy.*, 1994, **115**, 200–12.
18. McCall, John. Genetic algorithm for modeling and optimization. *J. Compu. Math.*, 2005, **184**.
19. Chung, H.S. & Alonso, J.J. Multiobjective optimization using approximation model-based genetic algorithm. *In* 10th AIAA/ISSMO, Multidisciplinary Analysis and Optimization Conference, Albany, NY, September 2004, AIAA Paper-2004-4325.
20. Yamazaki, Wataru; Matsushima, Kisa & Nakahashi, Kazuhiro. Aerodynamic shape optimization based on drag decomposition. *In* 24th Applied Aerodynamics Conference. AIAA Paper-2006-3332, 2006.
21. Myers, R.H. & Montgomery, D.C. Response surface methodology: process and product optimization using design experiments. Wiley, New York, 1978.
22. Ahn, J.K.; Kim, H.J.; Lee, D.H. & Rho, O.H. Response surface method for aircraft design in transonic flow. *Journal of Aircraft,* 2001, **38**(2), 231-38.
23. Sacks, Jerome; Welch, William J.; Mitchell, Toby J. & Wynn, Henry P. Design and analysis of computer experiments. *Statistical Science*, 1989, **4**(4), 409-35.
24. Simpson, Timothy W.; Mauery, Timothy M.; Korte, John J. & Mistree, Farrokh. Comparison of response surface and kriging models for multidisciplinary design optimization. AIAA Paper-1998-4755, 1998.
25. Jones, Donald R.; Schonlau, Matthias & Welch, William J. Efficient global optimization of expensive black-box function. *J. Global Optim.*, 1998, **13**, 455-92.
26. Mockus, J.; Tiesis, V. & Zilinskas, A. The application of bayesian methods for seeking the extremum. *Toward Global Optim.*, 1978, **2**, 117-29.
27. Jameson. Aerodynamic design via control theory. *J. Sci. Comput.*, 1988, **3**, 233-60,
28. Leoviriyakit, Kasidit & Jameson, Antony. Multi-point wing planform optimization via control theory. *In* 43rd Aerospace Science Meeting and Exhibit, 10-13 January 2005, Reno, Nevada. AIAA Paper-2005-0450.
29. Lee, B.J. & Kim, Chongam. Viscous aerodynamic shape optimization of wing/body configuration with overset mesh techniques. *In* Infotech@Aerospace 2007 Conference and Exhibit, Rohnert Park, California, 7-10 May 2007. AIAA Paper-2007-2872.
30. Piegl, L. & Tiller, W. The NURBS book. Springer. 1997.
31. Lee, B.J.; Kim, C.S.; Kim, Chongam; Rho, O.H. & Lee, K.D. Parallelized design optimization for transonic

wing using aerodynamic sensitivity analysis. AIAA Paper-2002-0264, 2002.

32. Vassberg, J.C.; Buning, P.G. & Rumsey, C.L. Drag prediction for the DLR-F4 wing/body using OVERFLOW and CFL3D on an overset mesh. AIAA Paper-2002-0840, 2002.
33. Yim, JinWoo; Lee, Byung Joon; Kim, Chongam & Obayashi, Shigeru. Multi-stage aerodynamic design of multi-body geometries by Kriging-based models and adjoint variable approach. *In* 26th AIAA Applied Aerodynamics Conference, Honolulu, Hawaii, 18-21 August 2008.

Contributor

Dr Chongam Kim is currently a Professor in the School of Mechanical and Aerospace Engineering at Seoul National University. He did his PhD in Aerospace Engineering from Princeton University, USA under the supervision of Antony Jameson His research interests include: Numerical methods for conservation laws, aerodynamic shape optimisation and flow control, compressible and cryogenic multi-phase flows, bio-mimetic aerodynamics and multi-disciplinary flow analysis.